Second-Order Cone Programming for Scan-Plane Reconstruction for the Wavelength-Scaled Array

W. Mark Dorsey, *Member, IEEE,* Jeffrey O. Coleman, *Senior Member, IEEE,* Rick W. Kindt, *Member, IEEE,* and Rashmi Mital

***Abstract*—The wavelength-scaled array architecture reduces the element count in large, ultrawideband antenna arrays by segmenting the aperture into subapertures of varying sizes and bandwidths. This results in an asymmetrical aperture of dissimilar elements with associated patterns that require significant correction. Here, we assess narrowband array performance using its far-field pattern as obtained in two steps. First, we characterize individual elements using planar near-field measurements. Second, we use second-order cone programming to optimize the complex element weights that generate the desired individual far-field element patterns derived from those measurements. This document details the far-field optimization technique, referred to here as optimized scan-plane reconstruction, and uses it to demonstrate that the asymmetric wavelength-scaled array can support low global sidelobe reduction, deep localized nulls, and/or mainbeam scanning like a conventional symmetric array.**

***Index Terms*—Calibration, Phased Arrays, Near-field far-field transformation, Antenna Measurement, Antenna Pattern Synthesis**

I. Introduction

The need for large ultrawideband arrays oftentimes leads to apertures that are oversampled at low frequency and larger than required at high frequency. The wavelength-scaled array (WSA) architecture reduces the overall element count by segmenting the aperture into subapertures consisting of elements of various sizes and bandwidths. This reduces the overall element count and produces relatively constant beamwidth as a function of frequency. The elements are scaled to operate over different bands within the overall frequency range, and subsequently the design results in an asymmetrical aperture. The performance of this array has been previously reported in [1]–[3], and it has been shown to provide a good impedance match and scan performance. Here we demonstrate the far-field performance beyond what has been reported previously by showing the ability of the WSA to form far-field beams with challenging sidelobe constraints and low taper loss.

This work details the theory of a unique array-pattern synthesis technique termed optimized scan-plane reconstruction. This technique uses the embedded near-field response of each element in an array environment sampled in a scan plane whose parameters are determined by the array aperture as described in [4]. We then superimpose the near-field responses using complex element weights and formulate a second-order cone program (SOCP) to optimize the far-field pattern with appropriate taper loss and sidelobe constraints. In an SOCP, the objective function is linear in the optimization variables and minimized subject to linear and second-order cone constraints [5]–[7]. The latter effectively upper bound nonnegative-definite quadratic functions of the variables, either by constants or by the squares of affine (linear plus a constant) functions of the variables. By using embedded near-field responses, the impact of inter-element interactions is included in this formulation.

The flexibility afforded by second-order cone constraints is ideal for our constrained taper-loss minimizations, and their software formulation is streamlined by our use of an NRL-developed toolbox [8] that serves as a front end to map high-level problem descriptions, in a Matlab environment, to various extraordinarily efficient, off-the-shelf numerical-optimization codes. The codes used here—our optimizations run fine using either—are SeDuMi [9], [10] and SDPT3 [11], [12].

The WSA is chosen for this demonstration because its irregular and asymmetrical arrangement of dissimilar elements make beamforming challenging. Optimized scan-plane reconstruction uses the element weights as optimization variables. A DFT relates the far-field patterns to those optimization variables for apertures of arbitrarily located dissimilar elements.

This paper first presents the theory of optimized scan-plane reconstruction and the SOCP formulation used in optimizing far-field patterns. This is followed by a brief description of the WSA architecture accompanied by optimized patterns. Here, the near-field distribution of each element is measured, and the presented far-field patterns are synthesized from those distributions.

II. Transforming the Near Field to the Far Field

Determining the far-field behavior of the complex electric field from PNF measurements is not new [13] but is reviewed here for completeness and to establish notation. The plane in which PNF data are taken is termed the scan plane throughout.

1) The Plane-Wave Spectrum: Mentally orient the scan plane vertically and view it edge-on with the antenna under test far enough to the left that evanescent fields are negligible in the right halfspace, the region on and to the right of the scan plane. At a point in the right halfspace given by vector $\mathbf{r}$ then, only propagating waves proportional to $\mathrm{e}^{-j\mathbf{k}\cdot\mathbf{r}}$ remain, where wavenumber vector $\mathbf{k}$ also lies in the right halfspace. Write $\mathbf{r} = \boldsymbol{\rho} + \mathbf{r}_\perp$ using components $\boldsymbol{\rho}$ and $\mathbf{r}_\perp$ in and normal to the scan plane respectively. Write wavenumber vector $\mathbf{k} = \boldsymbol{\kappa} + \mathbf{k}_\perp$ using in-plane and normal components. In visible region $\mathcal{V} = \{\boldsymbol{\kappa} : \|\boldsymbol{\kappa}\| \le \omega/c\}$, Helmholtz relation $\|\mathbf{k}\| = \omega/c$ determines $\mathbf{k}_\perp$ from $\boldsymbol{\kappa}$, making $\mathbf{k}$ a function of $\boldsymbol{\kappa}$. The complex electric field is superposition

$$\vec{E}(\mathbf{r}) = \frac{1}{2\pi}\int_{\mathcal{V}} \vec{f}(\boldsymbol{\kappa})\,\mathrm{e}^{-j\mathbf{k}\cdot\mathbf{r}}\,d\boldsymbol{\kappa} \tag{1}$$

with $d\boldsymbol{\kappa}$ differential area. Complex amplitude $\vec{f}(\boldsymbol{\kappa})$ is the plane-wave spectrum (PWS). Obtaining scan-plane component $\vec{f}_\parallel(\boldsymbol{\kappa})$ of $\vec{f}(\boldsymbol{\kappa}) = \vec{f}_\parallel(\boldsymbol{\kappa}) + \vec{f}_\perp(\boldsymbol{\kappa})$ from PNF data is detailed below. Set $\mathbf{k}\cdot\vec{f}(\boldsymbol{\kappa}) = 0$ to zero fields in the propagation direction and so fix normal component $\vec{f}_\perp(\boldsymbol{\kappa})$.

Manuscript received April 24, 2013. This work was supported by the Office of Naval Research.

The authors are with the Radar Division, U.S. Naval Research Laboratory, Washington, DC 20375, e-mail: wmdorsey@vt.edu.

2) The Far-Field Pattern: By a somewhat lengthy but classic derivation [13], the complex electric field $\vec{E}(r\hat{u})$ at point $r\hat{u}$ in the far field, a distance r away in the direction of right-halfspace unit vector $\hat{u}$, is a complex constant times phase-shift factor $\mathrm{e}^{-j\|\mathbf{k}\|r}$ times amplitude-rolloff factor $1/r$ times (arbitrarily scaled) antenna-pattern factor $\|\mathbf{k}_\perp\|\,\vec{f}(\boldsymbol{\kappa})$, where wavenumber $\mathbf{k} = \boldsymbol{\kappa} + \mathbf{k}_\perp$ points in the $\hat{u}$ direction. Henceforth we'll refer to direction $\boldsymbol{\kappa}$ to mean the direction of wavenumber $\mathbf{k}$ as determined by $\boldsymbol{\kappa}$, and, since for present purposes we are unconcerned with constant scale factors, we take the vector pattern in direction $\boldsymbol{\kappa}$ to be simply

$$\vec{A}(\boldsymbol{\kappa}) \triangleq \|\mathbf{k}_\perp\|\,\vec{f}(\boldsymbol{\kappa}). \tag{2}$$

3) The PWS and the PNF Fields are a 2D Transform Pair: In the $\mathbf{r}_\perp = 0$ scan plane where $\mathbf{k}\cdot\mathbf{r} = \boldsymbol{\kappa}\cdot\boldsymbol{\rho}$, the integral formulation in (1) is just 2D Fourier transform

$$\vec{E}(\boldsymbol{\rho}) = \frac{1}{2\pi}\int 1_{\mathcal{V}}(\boldsymbol{\kappa})\vec{f}(\boldsymbol{\kappa})\,\mathrm{e}^{-j\boldsymbol{\kappa}\cdot\boldsymbol{\rho}}\,d\boldsymbol{\kappa}$$

where indicator function $1_{\mathcal{V}}(\boldsymbol{\kappa})$ is unity for $\boldsymbol{\kappa}\in\mathcal{V}$ and zero elsewhere. PNF fields determine $\vec{f}(\boldsymbol{\kappa})$ through inverse

$$1_{\mathcal{V}}(\boldsymbol{\kappa})\vec{f}(\boldsymbol{\kappa}) = \frac{1}{2\pi}\int \vec{E}(\boldsymbol{\rho})\,\mathrm{e}^{j\boldsymbol{\kappa}\cdot\boldsymbol{\rho}}\,d\boldsymbol{\rho}.$$

Likewise, for scan-plane components of $\vec{f}(\boldsymbol{\kappa})$ and $\vec{E}(\boldsymbol{\rho})$,

$$1_{\mathcal{V}}(\boldsymbol{\kappa})\vec{f}_{\parallel}(\boldsymbol{\kappa}) = \frac{1}{2\pi}\int \vec{E}_{\parallel}(\boldsymbol{\rho})\,\mathrm{e}^{j\boldsymbol{\kappa}\cdot\boldsymbol{\rho}}\,d\boldsymbol{\rho}. \tag{3}$$

4) Sampling the Scan Plane: Use the columns of 3×2 matrix $\mathbf{B}$ as lattice basis vectors and synthesize

$$\vec{E}^{s}_{\parallel}(\boldsymbol{\rho}) \triangleq \sum_{\substack{\boldsymbol{n}\in\mathbb{Z}^2\\ \text{as columns}}} \vec{d}_{\boldsymbol{n}}\,\delta(\boldsymbol{\rho}-\mathbf{B}\boldsymbol{n}) \tag{4}$$

using PNF field data taken at the lattice points:

$$\vec{d}_{\boldsymbol{n}} \triangleq |\mathbf{B}^T\mathbf{B}|^{1/2}\,\vec{E}_{\parallel}(\mathbf{B}\boldsymbol{n}).$$

Replace $\vec{E}_{\parallel}(\boldsymbol{\rho})$ in (3) with $\vec{E}^{s}_{\parallel}(\boldsymbol{\rho})$ of (4) and convolve the left side of (3) with unit impulses on the dual lattice. Let $\boldsymbol{\kappa}$ be a row vector and use pseudoinverse $\mathbf{B}^{+}\triangleq(\mathbf{B}^T\mathbf{B})^{-1}\mathbf{B}^T$. Then

$$\sum_{\substack{\boldsymbol{m}\in\mathbb{Z}^2\\ \text{as rows}}} 1_{\mathcal{V}}(\boldsymbol{\kappa}-\boldsymbol{m}\mathbf{B}^{+})\,\vec{f}_{\parallel}(\boldsymbol{\kappa}-\boldsymbol{m}\mathbf{B}^{+}) = \frac{1}{2\pi}\int \sum_{\substack{\boldsymbol{n}\in\mathbb{Z}^2\\ \text{as columns}}} \vec{d}_{\boldsymbol{n}}\,\delta(\boldsymbol{\rho}-\mathbf{B}\boldsymbol{n})\,\mathrm{e}^{j\boldsymbol{\kappa}\boldsymbol{\rho}}\,d\boldsymbol{\rho}.$$

Choose lattice basis $\mathbf{B}$ so that the nearest-neighbor distance in the dual lattice exceeds $2\omega/c$, the diameter of visible region $\mathcal{V}$. Then the terms on the left do not overlap. Restrict $\boldsymbol{\kappa}$ to a set in which all $\boldsymbol{m}\neq 0$ terms on the left are zero, a set that includes visible region $\mathcal{V}$. Integrating on the right then yields

$$\vec{f}_{\parallel}(\boldsymbol{\kappa}) = \frac{1}{2\pi}\sum_{\substack{\boldsymbol{n}\in\mathbb{Z}^2\\ \text{as columns}}} \vec{d}_{\boldsymbol{n}}\,\mathrm{e}^{j\boldsymbol{\kappa}\mathbf{B}\boldsymbol{n}}. \tag{5}$$

5) Sample Wavenumber Space to Compute: Restrict $\boldsymbol{\kappa}$ further to a point lattice by setting $\boldsymbol{\kappa} = -(2\pi/N)\boldsymbol{k}''\mathbf{B}^{-1}$. Choose integer N to obtain the desired point density. Then write row index vector $\boldsymbol{k}''$ uniquely as $\boldsymbol{k}'' = \boldsymbol{k}'N + \boldsymbol{k}$. Use modulo-$N$ operations to obtain $\boldsymbol{k}\in\{0,\ldots,(N-1)\}^2$, and then solve for $\boldsymbol{k}'\in\mathbb{Z}^2$. Sampling relationship

$$\boldsymbol{\kappa} = -(2\pi/N)(\boldsymbol{k}'N+\boldsymbol{k})\mathbf{B}^{-1} \tag{6}$$

makes complex exponential $\mathrm{e}^{j\boldsymbol{\kappa}\mathbf{B}\boldsymbol{n}}$ in (5) just $\mathrm{e}^{-2\pi j\boldsymbol{k}\boldsymbol{n}/N}$, so

$$\vec{f}_{\parallel}(\boldsymbol{\kappa}) = \frac{1}{2\pi}\sum_{\substack{\boldsymbol{n}\in\mathbb{Z}^2\\ \text{as columns}}} \vec{d}_{\boldsymbol{n}}\,\mathrm{e}^{-2\pi j\boldsymbol{k}\boldsymbol{n}/N}. \tag{7}$$

6) Decompose the Element Index Modulo N for a DFT: Replace $\boldsymbol{n}$ with $\boldsymbol{n}''$ throughout (7), and forget $\boldsymbol{n}$ ever existed. Set $\boldsymbol{n}'' = N\boldsymbol{n}' + \boldsymbol{n}$ to split the sum into a double sum over $\boldsymbol{n}'\in\mathbb{Z}^2$ and $\boldsymbol{n}\in\{0,\ldots,(N-1)\}^2$. On the $\boldsymbol{\kappa}$ of (6) then,

$$\vec{f}_{\parallel}(\boldsymbol{\kappa}) = \frac{1}{2\pi}\sum_{\substack{\boldsymbol{n}\in\{0,\ldots,(N-1)\}^2\\ \text{as columns}}} \left(\sum_{\boldsymbol{n}'\in\mathbb{Z}^2 \text{ as cols}} \vec{d}_{N\boldsymbol{n}'+\boldsymbol{n}}\right)\mathrm{e}^{-j2\pi\boldsymbol{k}\boldsymbol{n}/N}.$$

The outer sum is a 2D discrete Fourier transform (DFT) of the parenthesized quantity, which is indexed on $\boldsymbol{n}$. Truncating the PNF scan plane makes the inner sum finite. Choose a highly composite N for efficient computation with an FFT.

Where the Scan Plane is Truncated: PNF data are taken on a scan plane that is actually too small to permit accurate size element patterns to be computed, but the scan plane is sized appropriately for the array aperture as a whole, so element-level scan-plane truncation errors cancel sufficiently in beamforming to give accurate array-level results.

III. Optimized Scan-Plane Reconstruction

In this work PNF measurements are never actually made on an operating array. Instead, since the fields are linear in the element inputs, the missing array PNF data are assumed to be just the element-level PNF data combined using the vector $\mathbf{w} = [w_\ell]$ of L complex beamforming weights as on the left in Fig. 1. The PWS is linear in the PNF data, so the array PWS is a similarly weighted combination of the element plane-wave spectra, as on the right in Fig. 1. The element plane-wave spectra are determined by corresponding element-level PNF data, represented at the top in Fig. 1 and discussed above in Section II. The array PWS, as inferred in this way from weight vector $\mathbf{w}$ and element-level PNF data, then determines array transmit pattern $\vec{A}(\boldsymbol{\kappa})$ of (2).

Here we optimize weight vector $\mathbf{w}$ to minimize the equivalent receive pattern's taper loss subject to sidelobe constraints. The SOCP formulation generalizes an earlier one [7], [14]–[16] to permit nonidentical element patterns and to apply sidelobe nulling to arbitrarily polarized signals.

A. Taper Loss for Nonidentical Elements

The simplest way to derive taper loss is as the degradation in the receive signal-to-noise ratio (SNR) relative to the best obtainable with any choice of weights.

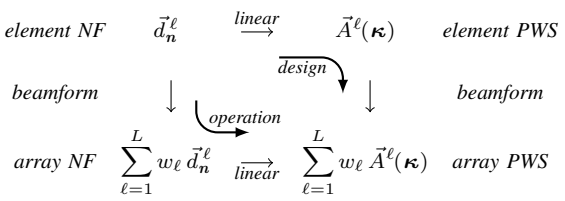

Fig. 1. Element-level PNF data at sample points $n = 1 \cdots N$(upper left) measured for elements $\ell = 1 \ldots L$ determine the array PWS (lower right) differently in design and operation, but linearity makes that irrelevant. Here w_ℓ is the ℓth complex element weight and $\boldsymbol{\kappa}$ represents propagation direction.

For signals transmitted and received along the mainbeam direction, let the vector wavenumber have scan-plane components of $\boldsymbol{\kappa}_0$ and $-\boldsymbol{\kappa}_0$ respectively, and for simplicity call that direction the $\boldsymbol{\kappa}_0$ direction. Let p_ℓ^* be the complex co-pol receive pattern of element ℓ in that direction, i.e. the complex amplitude of the output of element ℓ in response to a far-field co-pol signal from that direction of some hypothetical standard complex amplitude. The array output amplitude in response to that signal is then $\sum_{\ell=1}^{L} w_\ell p_\ell^* = \langle \mathbf{w}, \mathbf{p}_0 \rangle$, where the vectors of length L given by $\mathbf{w} \triangleq [w_\ell]$ and $\mathbf{p}_0 \triangleq [p_\ell]$ gather the constants together. If we assume that elements have identical, individual LNAs that determine the level of complex noise they contribute to element outputs, the complex noise power at the array output is proportional to $\sum_\ell |w_\ell|^2 = \|\mathbf{w}\|^2$. The SNR as a power ratio—call it SNR^2—is therefore proportional to $|\langle \mathbf{w}, \mathbf{p}_0 \rangle|^2 / \|\mathbf{w}\|^2$. We can introduce a convenient scaling by including a proportionality constant of $1/\|\mathbf{p}_0\|^2$ and defining

$$\text{SNR}^2 = \frac{|\langle \mathbf{w}, \mathbf{p}_0 \rangle|^2}{\|\mathbf{w}\|^2 \|\mathbf{p}_0\|^2}. \tag{8}$$

The convenience of this scaling arises from the Schwartz inequality, which upper bounds this quantity by unity. Setting $\mathbf{w} = \mathbf{p}_0$ and substituting $\langle \mathbf{p}_0, \mathbf{p}_0 \rangle = \|\mathbf{p}_0\|^2$ in the above shows that the bound can in fact be met with equality, making this a measure of SNR relative to the best achievable.

B. SNR Maximization Subject to Point Pattern Bounds

1) A Point Pattern Bound for Arbitrary Polarization: The array's co- and cross-pol complex receive patterns take forms $\langle \mathbf{w}, \mathbf{p} \rangle$ and $\langle \mathbf{w}, \mathbf{q} \rangle$ respectively for some complex vectors $\mathbf{p}$ and $\mathbf{q}$ that are both functions of direction $\boldsymbol{\kappa}$. So far, so good, but for arbitrary polarization we need more precise statements.

Suppose far-field signals of our hypothetical standard complex amplitude are incident on the array from direction $\boldsymbol{\kappa}$, resulting in co- and cross-pol scan-plane fields proportional to $\hat{c}\, \mathrm{e}^{j\boldsymbol{\kappa}\cdot\boldsymbol{\rho}}$ and $\hat{x}\, \mathrm{e}^{j\boldsymbol{\kappa}\cdot\boldsymbol{\rho}}$ for some complex unit vectors $\hat{c}$ and $\hat{x}$, both functions of $\boldsymbol{\kappa}$, that define co and cross polarizations. The resulting complex array-output signal amplitudes, samples of the array's co- and cross-pol complex receive patterns for direction $\boldsymbol{\kappa}$, are $\langle \mathbf{w}, \mathbf{p} \rangle$ and $\langle \mathbf{w}, \mathbf{q} \rangle$ respectively. An standard-amplitude incident wave of scan-plane form $\hat{p}\, \mathrm{e}^{j\boldsymbol{\kappa}\cdot\boldsymbol{\rho}}$, where polarization unit vector $\hat{p}$ is arbitrary, then yields complex array-output amplitude

$$R \triangleq \langle \hat{p}, \hat{c} \rangle \langle \mathbf{w}, \mathbf{p} \rangle + \langle \hat{p}, \hat{x} \rangle \langle \mathbf{w}, \mathbf{q} \rangle. \tag{9}$$

This uses unit-vector inner products in a complex threespace and bold-vector inner products in complex L space. An inner product is conjugate linear in its second argument: $\langle \mathbf{u}, a_1 \mathbf{v}_1 + a_2 \mathbf{v}_2 \rangle = a_1^* \langle \mathbf{u}, \mathbf{v}_1 \rangle + a_2^* \langle \mathbf{u}, \mathbf{v}_2 \rangle$. So (9) is equivalent to

$$\begin{aligned} R &= \langle \hat{p}, \vec{A} \rangle \\ \vec{A} &\triangleq \langle \mathbf{w}, \mathbf{p} \rangle^* \hat{c} + \langle \mathbf{w}, \mathbf{q} \rangle^* \hat{x}. \end{aligned} \tag{10}$$

Here both $\mathbf{p}$ and $\mathbf{q}$ depend on direction $\boldsymbol{\kappa}$ and therefore so does array pattern $\vec{A}$, even though the dependency is not shown.

To upper bound $|R|$ for arbitrary $\hat{p}$, we upper bound $\max_{\hat{p}} |\langle \hat{p}, \vec{A} \rangle|$, which by the Schwartz inequality is just $\|\vec{A}\|$. By (10) bound $\|\vec{A}\| \le b$ can be written, assuming $b > 0$, as

$$\|\langle \mathbf{w}, \mathbf{p} \rangle^* \hat{c} + \langle \mathbf{w}, \mathbf{q} \rangle^* \hat{x}\|^2 \le b^2$$

or the equivalent, if we expand the squared norm,

$$|\langle \mathbf{w}, \mathbf{p} \rangle|^2 + 2Re\{\langle \mathbf{w}, \mathbf{p} \rangle^* \langle \mathbf{w}, \mathbf{q} \rangle \langle \hat{c}, \hat{x} \rangle\} + |\langle \mathbf{w}, \mathbf{q} \rangle|^2 \le b^2.$$

Orthogonal polarization vectors simplify. If $\langle \hat{c}, \hat{x} \rangle = 0$, it's just

$$|\langle \mathbf{p}, \mathbf{w} \rangle|^2 + |\langle \mathbf{q}, \mathbf{w} \rangle|^2 \le b^2.$$

2) A Second-Order Cone Program: Let us use the arbitrary-polarization point pattern bound developed above, but with subscripts $i = 1, 2, \ldots N_c$ up to some limit representing distinct sidelobe directions of interest. The value of N_c depends upon the pattern shape, the size of the constrained region, and the desired bound limit. Careful attention should be made to check the constraint definitions to ensure accurate results. As before, write the array's mainbeam-direction complex co-pol receive pattern $\langle \hat{c}(\boldsymbol{\kappa}_0), \vec{A}(\boldsymbol{\kappa}_0) \rangle$ as $\langle \mathbf{w}, \mathbf{p}_0 \rangle$. Then consider the SOCP

$$\begin{aligned} &\textit{Optimize} \text{ real variable } \Lambda \text{ and complex vector } \mathbf{w} \\ &\textit{to minimize } \Lambda \\ &\textit{subject to} \text{ noise constraint } \|\mathbf{w}\| \|\mathbf{p}_0\| \le \Lambda, \\ &\qquad \text{mainbeam constraint } \mathrm{Re}(\langle \mathbf{w}, \mathbf{p}_0 \rangle) \ge 1, \\ &\qquad \textit{and} \text{ point bound } \sqrt{|\langle \mathbf{w}, \mathbf{p}_i \rangle|^2 + |\langle \mathbf{w}, \mathbf{q}_i \rangle|^2} \le b_i \\ &\qquad \text{for each of } i = 1, 2, \ldots, N_c \end{aligned} \tag{11}$$

Arguing that this SOCP does what we want requires two steps.

First, Λ appears only in the noise constraint, so if during optimization that constraint does not hold with equality, Λ can be immediately reduced until it does, thereby harmlessly improving the objective. The optimization must end with $\|\mathbf{w}\| \|\mathbf{p}_0\| = \Lambda$, so minimizing Λ effectively minimizes $\|\mathbf{w}\|$.

Second, suppose that at some point all constraints are satisfied. The mainbeam constraint implies $|\langle \mathbf{w}, \mathbf{p}_0 \rangle| \ge 1$ or its equivalent $|\langle \mathbf{w}, \mathbf{p}_0 \rangle|^{-1} \le 1$, so let us replace $\mathbf{w}$ with

$$\mathbf{w}_{\text{new}} = \frac{1}{\langle \mathbf{w}, \mathbf{p}_0 \rangle} \mathbf{w}.$$

This replacement yields objective

$$\Lambda_{\text{new}} = \|\mathbf{w}_{\text{new}}\| \|\mathbf{p}_0\| = \frac{\|\mathbf{w}\| \|\mathbf{p}_0\|}{|\langle \mathbf{w}, \mathbf{p}_0 \rangle|} \le \|\mathbf{w}\| \|\mathbf{p}_0\| = \Lambda$$

so optimization progress is unharmed. Further,

$$|\langle \mathbf{w}_{\text{new}}, \mathbf{p}_i \rangle| = \left| \frac{\langle \mathbf{w}, \mathbf{p}_i \rangle}{\langle \mathbf{w}, \mathbf{p}_0 \rangle} \right| \le |\langle \mathbf{w}, \mathbf{p}_i \rangle|,$$

$$|\langle \mathbf{w}_{\text{new}}, \mathbf{q}_i \rangle| = \left| \frac{\langle \mathbf{w}, \mathbf{q}_i \rangle}{\langle \mathbf{w}, \mathbf{p}_0 \rangle} \right| \le |\langle \mathbf{w}, \mathbf{q}_i \rangle|$$

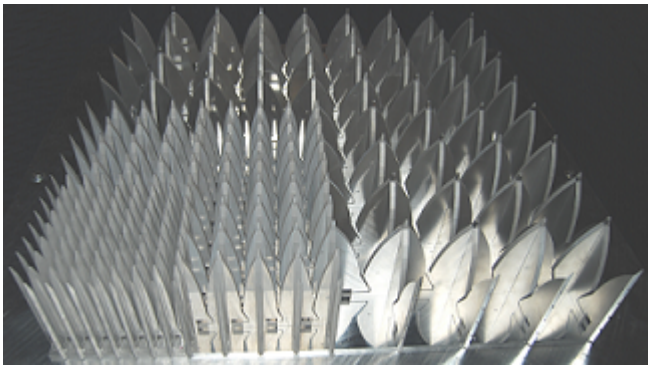

Fig. 2. Photograph of Ultrawideband Wavelength-Scaled Array (WSA)

for $i = 1, 2, \ldots, N_c$, so the point bounds in (11) are still met:

$$|\langle \mathbf{w}_{\text{new}}, \mathbf{p}_i \rangle|^2 + |\langle \mathbf{w}_{\text{new}}, \mathbf{q}_i \rangle|^2 \leq |\langle \mathbf{w}, \mathbf{p}_i \rangle|^2 + |\langle \mathbf{w}, \mathbf{q}_i \rangle|^2 \leq b_i^2.$$

The mainbeam constraint in (11) is likewise still met, because

$$\langle \mathbf{w}_{\text{new}}, \mathbf{p}_0 \rangle = \frac{\langle \mathbf{w}, \mathbf{p}_0 \rangle}{\langle \mathbf{w}, \mathbf{p}_0 \rangle} = 1.$$

Finally, the latter result lets us write $\Lambda_{\text{new}} = \|\mathbf{w}_{\text{new}}\|\|\mathbf{p}_0\|$ as

$$\Lambda_{\text{new}} = \frac{\|\mathbf{w}_{\text{new}}\|\|\mathbf{p}_0\|}{\langle \mathbf{w}_{\text{new}}, \mathbf{p}_0 \rangle}$$

and (8) then shows that $1/\Lambda_{\text{new}}^2 = \text{SNR}^2$. It follows that $20 \log_{10} \Lambda$ is dB taper loss.

By the above, an optimum weight vector $\mathbf{w}$ with respect to the following is also optimum with respect to SOCP (11):

$$\begin{aligned} &\textit{Optimize} \text{ complex weight vector } \mathbf{w} \\ &\textit{to minimize} \text{ dB taper loss} \\ &\quad \textit{subject to} \text{ mainbeam constraint } \langle \hat{c}(\boldsymbol{\kappa}_0), \vec{A}(\boldsymbol{\kappa}_0) \rangle = 1 \\ &\qquad \textit{and} \text{ bound } \max_{\hat{p}} |\langle \hat{p}, \vec{A}(\boldsymbol{\kappa}_i) \rangle| \leq b_i \text{ for } i = 1, 2, \ldots, N_c \end{aligned} \tag{12}$$

SOCP (11) typically has a unique optimal $\mathbf{w}$, in which case it is also the unique optimum of this program. Of course mathematical program (12) is what we wish to optimize. We use SOCP (11) instead because we have the tools to do so.

IV. Wavelength-Scaled Array Performance

In this paper, we apply a SOCP formulation to reconstruct the scan-plane of the the dual-polarized WSA prototype [1] shown in Fig. 2 radiating at 2.0 GHz. At this frequency, all elements of the array are well matched over wide scan angles. Coherent, phase-locked pattern data are measured for each element using identical sampling grids to allow application of the scan plane reconstruction technique [4]. Since it was not possible to simultaneously measure all the elements at once, it was crucial that the measurement system remained stationary—both electrically and mechanically—for the duration of the measurement-collection process.

The data used in this paper was collected for only a single-polarization—defined here as vertically polarized (V-pol)—with the orthogonally polarized elements (H-pol) terminated in a 50Ω load. These polarization conventions follow Ludwig's third definition of polarization in [17]. The H- and V-pol

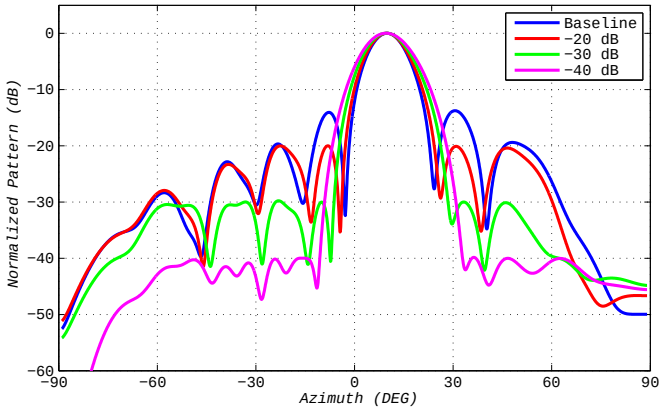

(a) Azimuth Pattern ($\theta_{\text{el}} = 0$)

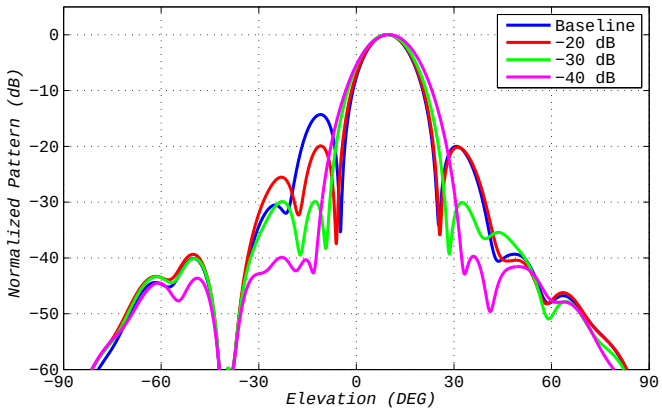

(b) Elevation Pattern ($\theta_{\text{az}} = 0$)

Fig. 3. Optimized radiation patterns of the wavelength-scaled array with main beam scanned to $(\theta_{\text{az}}, \theta_{\text{el}}) = (10°, 10°)$ subject to varying sidelobe constraints.

pattern of the WSA optimized with only a taper-loss constraint is shown in Fig. 5. This optimization resulted in $\Lambda = 0.00dB$.

Fig. 3 shows the pattern magnitude for the WSA optimized to minimize taper loss Λ with the main beam scanned to $(\theta_{\text{az}}, \theta_{\text{el}}) = (10°, 10°)$ subject to sidelobe constraints imposed in two regions defined as $\mathcal{K}_{\text{notch}}$ and $\mathcal{K}_{\text{sl}}$. We use $\mathcal{K}_{\text{notch}}$ to impose constraints for a deeply suppressed notch region for $-42° \leq \theta_{\text{el}} \leq -38°$. Following the SOCP formulation from (12), we constrain the sidelobes using $20 \log|\vec{f}(\boldsymbol{\kappa}_i)| \leq -60$ dB for $\boldsymbol{\kappa}_i \in \mathcal{K}_{\text{notch}}$. Set $\mathcal{K}_{\text{sl}}$ contains the entire visible region exluding the main beam and $\mathcal{K}_{\text{notch}}$. We globally restrict the sidelobe levels below a desired bound using $|\vec{f}(\boldsymbol{\kappa}_i)| \leq B$ for $\boldsymbol{\kappa}_i \in \mathcal{K}_{\text{sl}}$, and B is varied from -20 dB to -40 dB in Fig. 3. The results are compared to the baseline pattern which is optimized to minimize taper loss Λ, scan the main beam to $(\theta_{\text{az}}, \theta_{\text{el}}) = (10°, 10°)$, and constrain the sidelobes within the null region $\mathcal{K}_{\text{notch}}$. The volumetric pattern for the case with $B = -30$ dB and associated constraint locations are shown in Fig. 6.

The optimized patterns shown in Fig. 3 use 161 constraints in the nulled region $\mathcal{K}_{\text{notch}}$, but the number of constraints required in $\mathcal{K}_{\text{sl}}$ varies with the constraint level B. As the sidelobe constraint level decreases, the main beam of the optimized pattern broadens, and the inner radius of $\mathcal{K}_{\text{sl}}$ increases,

TABLE I
TAPER LOSS (Λ) AND NUMBER OF CONSTRAINTS (N_c) FOR SIDELOBE LEVEL OPTIMIZATIONS OF FIG. 3

SLL	00 dB	−20 dB	−30 dB	−40 dB
Λ	0.83 dB	1.00 dB	1.52 dB	2.34 dB
N_c	161	3640	3456	3372

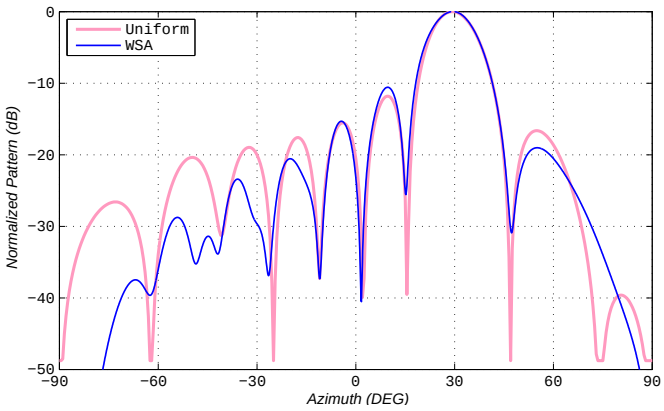

Fig. 4. Comparison between the optimized pattern of the wavelength-scaled array to an ideal array of similar elements.

subsequently decreasing the number of required constraints. Table I lists the computed Λ and number N_c of sidelobe constraints for each beam design.

It should be noted that—because these patterns are optimized from measured PNF results—they are subject to PNF measurement uncertainties. This is most notable in the pattern for -40 dB sidelobe constraints where the measurement system dynamic range is becoming a limiting factor in the achievable null depths. This sidelobe level performance would be difficult to realize in a practical system because the optimization is trying to meet sidelobe constraints while correcting measurement errors that would not exist in a true system. A thorough error analysis on the measurement system following the familiar NIST 18-term error budget [18] is recommended prior to measurements to provide an understanding of the limitations for a given measurement system.

Although it has nonuniform elements distributed assymetrically, the WSA is able to approach the performance of an array of uniformly distributed similar elements. In Fig. 4, the pattern of the WSA optimized with only a taper-loss constraint is compared to that of a uniform array of similar elements for a beam scanned to $(\theta_{\text{az}}, \theta_{\text{el}}) = (30°, 0°)$. The uniform array used in this has an aperture equal in size to that of the WSA, but with elements spaced on a square lattice with element separation of $\lambda/2$ and having a $\cos(\theta)$ element pattern. The results indicate that the optimization procedure presented in this paper can bring the WSA performance into close agreement with the pattern of an ideal array. All of the optimizations discussed in this paper were completed in less than a minute on a typical desktop computer.

V. CONCLUSION

This paper describes an array pattern synthesis technique that uses a second-order cone program (SOCP) formulation to optimize far-field patterns from element-level near-field responses. The beamforming process optimizes complex element weights by minimizing taper loss subject to various sidelobe constraints. The optimization technique is applied to the wavelength-scaled array (WSA), which is an interesting application due to its irregularly spaced nonuniform elements. The results shown in this paper indicate that the WSA can efficiently scan its main beam while reducing sidelobes—either globally or in deeply suppressed null regions. The performance of the wavelength-scaled array verifies its potential to reduce the element count and associated cost of large, ultrawideband radiators without sacrificing performance.

REFERENCES

[1] R. Kindt, "Prototype design of a modular ultrawideband wavelength-scaled array of flared notches," *IEEE Trans. Antennas Propag.*, vol. 60, no. 3, pp. 1320–1328, Mar. 2012.
[2] R. Kindt and M. Vouvakis, "Analysis of a wavelength-scaled array (WSA) architecture," *IEEE Trans. Antennas Propag.*, vol. 58, no. 9, pp. 2866 –2874, Sep. 2010.
[3] R. Kindt and M. Kragalott, "A wavelength-scaled ultra-wide bandwidth array," in *IEEE AP-S Int'l Symp.*, Jun. 2009, pp. 1 –4.
[4] A. Sayers, W. Dorsey, K. O'Haver, and J. Valenzi, "Planar near-field measurement of digital phased arrays using near-field scan plane reconstruction," *IEEE Trans. Antennas Propag.*, vol. 60, no. 6, pp. 2711–2718, Jun. 2012.
[5] M. S. Lobo, L. Vandenberghe, S. Boyd, and H. Lebret, "Applications of second-order cone programming," *Linear Algebra and its Applications*, vol. 284, pp. 193–228, Nov. 1998.
[6] J. Coleman and D. Scholnik, "Design of nonlinear-phase FIR filters with second-order cone programming," in *IEEE Midwest Symp. on Circuits and Systems*, Aug. 1999.
[7] D. P. Scholnik and J. O. Coleman, "Optimal array-pattern synthesis for wideband digital transmit arrays," *IEEE Journal on Selected Topics in Signal Processing*, vol. 1, no. 4, pp. 660–677, Dec. 2007.
[8] J. Coleman, D. Scholnik, and J. Brandriss, "A specification language for the optimal design of exotic FIR filters with second-order cone programs," in *IEEE Asilomar Conf. on Signals, Systems, and Computers*, Nov. 2002, a preprint is recommended, as the IEEE version is corrupted.
[9] J. F. Sturm, "Using SeDuMi 1.02, a Matlab toolbox for optimization over symmetric cones," *Optimization Methods and Software*, vol. 11–12, pp. 625–653 (versions 1.02/1.03), 1999, updated for version 1.05 online in 2001 (http://www.optimization-online.org/DB_HTML/2001/10/395.html).
[10] I. Pólik and T. Terlaky. SeDuMi 1.21. Cor@l Lab: Computational Optimization Research at Lehigh (http://sedumi.ie.lehigh.edu/).
[11] R. H. Tütüncü, K. C. Toh, and M. J. Todd, "Solving semidefinite-quadratic-linear programs using SDPT3," *Mathematical Programming*, vol. 95, no. 2, pp. 189–217, Feb. 2003. [Online]. Available: http://dx.doi.org/10.1007/s10107-002-0347-5
[12] K. C. Toh, M. Todd, and R. H. Tütüncü, "SDPT3 – a MATLAB software package for semidefinite programming," *Optimization Methods and Software*, vol. 11, pp. 545–581, 1999.
[13] J. J. H. Wang, "An examination of the theory and practices of planar near-field measurement," *IEEE Trans. Antennas Propag.*, vol. 36, no. 6, pp. 746–753, Jun. 88.
[14] J. O. Coleman, D. P. Scholnik, and P. E. Cahill, "Synthesis of a polarization-controlled pattern for a wideband array by solving a second-order cone program," in *IEEE AP-S Int'l Symp.*, Jul. 2005.
[15] J. O. Coleman, "Tapers for large planar phased arrays on regular grids: simple design methods versus second-order cone programming," in *European Signal Processing Conf*, Aug. 2010.
[16] ——, "Nonseparable Nth-band filters as overlapping-subarray tapers," in *IEEE Radar Conf.*, May 2011.
[17] A. Ludwig, "The definition of cross polarization," *IEEE Trans. Antennas Propag.*, vol. 21, no. 1, pp. 116–119, 1973.
[18] A. Newell, "Error analysis techniques for planar near-field measurements," *IEEE Trans. Antennas Propag.*, vol. 36, no. 6, pp. 754–768, Jun. 1988.

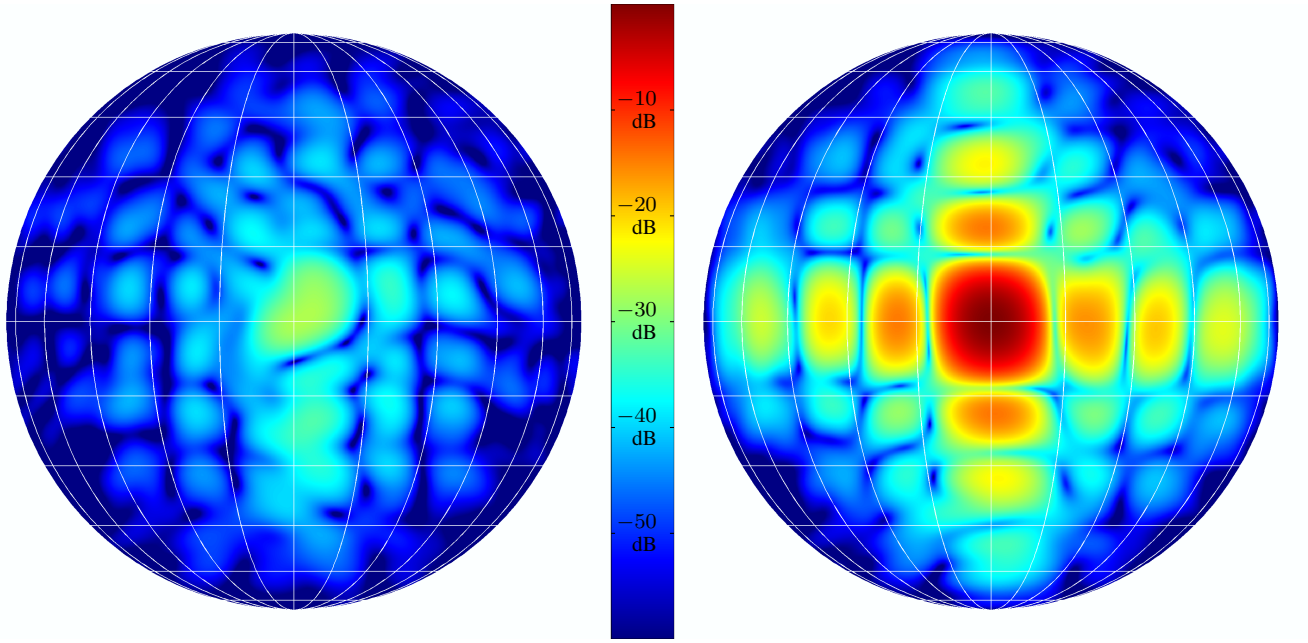

Fig. 5. H-pol (left) and total power (right) pattern of wavelength-scaled array optimized to minimize taper loss. (Taper loss $\Lambda = 0.00$ dB)

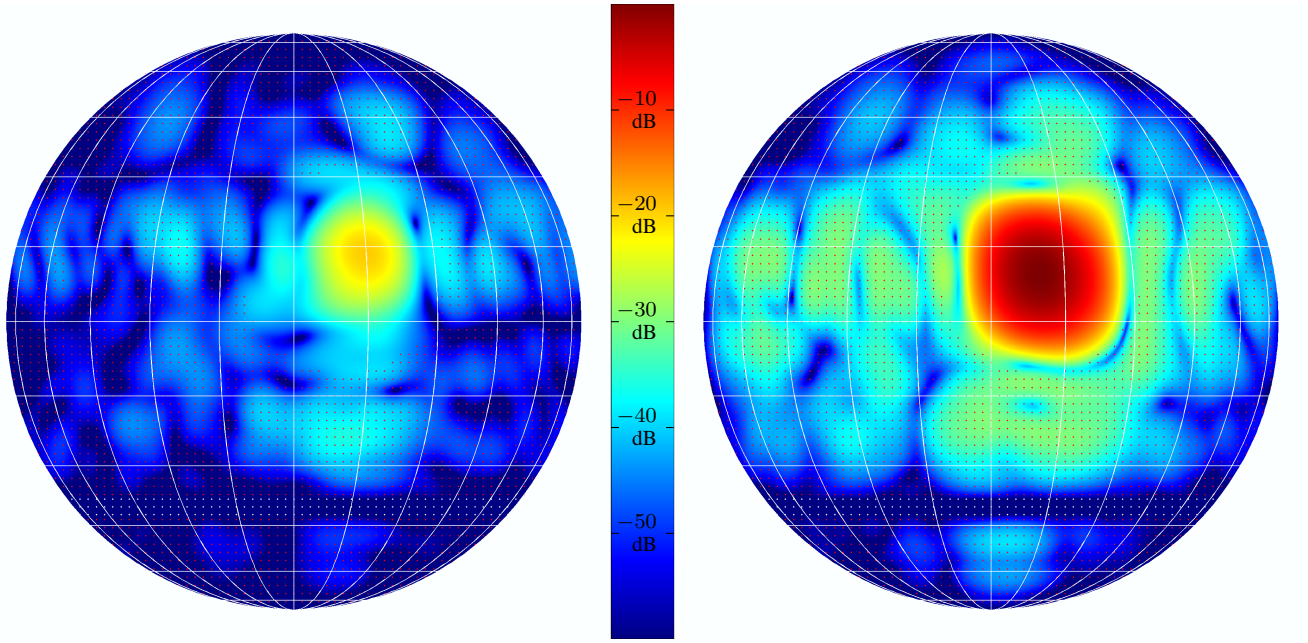

Fig. 6. H-pol (left) and total power (right) pattern of wavelength-scaled array optimized to minimize taper loss and scan main beam to $(\theta_{\text{az}}, \theta_{\text{el}}) = (10^\circ, 10^\circ)$ subject to sidelobe constraints that form a null over $-42^\circ \leq \theta_{\text{el}} \leq -38^\circ$ and reduce sidelobes below -30 dB. (Taper loss $\Lambda = 1.52$ dB). The location of the null region point constraints and sidelobe level point constraints appear as white and red dots respectively.